Excitonic Probe for Characterization of High-Quality Quantum-Well Heterostructures

P. Yu. Shapochkin,[1] S.A. Eliseev,[1] V.A. Lovtcius,[1] Yu. P. Efimov,[1] P.S. Grigoryev,[2,*]
E.S. Khramtsov,[2] and I.V. Ignatiev[2]

[1] *Department of Physics, St. Petersburg State University, Ulyanovskaya 1, Petrodvorets, St. Petersburg 198504, Russia*

[2] *Spin Optics Laboratory, St. Petersburg State University, Ulyanovskaya 1, Petrodvorets, St. Petersburg 198504, Russia*

(Received 30 April 2019; revised manuscript received 10 July 2019; published 17 September 2019)

High-quality GaAs/(Al, Ga)As heterostructures with quantum wells grown by molecular-beam-epitaxy technology are experimentally studied by means of optical spectroscopy of exciton states. The exciton resonances observed in the reflectance spectra are analyzed in the framework of phenomenological and microscopic models. The exciton energies, the radiative ($\hbar\Gamma_0$) and nonradiative ($\hbar\Gamma$) broadening, and the phases of resonant reflection are obtained from the modeling for each exciton resonance. These parameters are used for careful analysis of the parameters and quality of the structures. Particular attention is paid to the exciton energies and phases, which are used to determine the quantum-well and barrier-layer thicknesses with high accuracy.

DOI: 10.1103/PhysRevApplied.12.034034

I. INTRODUCTION

The technology of molecular beam epitaxy (MBE) allows one to grow semiconductor heterostructures of exceptional quality, with ultralow levels of impurity defects and perfect morphology. The record quality achieved for GaAs-based structures in particular is the basis of many applications [1]. The top level is probably achieved in designing quantum cascade lasers (QCLs) for the terahertz spectral range [2–4], and polaritonic devices based on microcavity (MC) structures [5]. In addition to high quality, QCL and MC structures require precise control of the layer thicknesses of the structure to an accuracy of about 1% [6,7].

The quality of direct-gap III-V structures can be characterized optically by photoluminescence (PL) and/or reflectance spectroscopy. High-quality structures exhibit a high PL quantum yield and narrow exciton lines [8,9]. Yet these are rather qualitative characteristics. Strict quantitative characteristics of the quality of the structure are provided by reflectance spectroscopy [10–14]. Continuously improving the quality of MBE-grown heterostructures imposes increasingly strict requirements on the accuracy of their optical characterization.

The basic principles of MBE technology are well described, e.g., in Refs. [1,16–19]. Several technological parameters have to be optimized to obtain a good crystal structure in an epitaxial layer. The most important of them are the substrate temperature, the growth rate, and the arsenic-to-metal (Ga, Al, or In) ratio set by the beam-equivalent pressures (BEPs). For each type of layer, say for GaAs and AlAs layers, these parameters differ, and therefore adjustment of them is required to grow any particular structure. The quality of the interfaces of the layers is also sensitive to these parameters. To prevent the growth of dislocations from the substrate into the structure, "technological" layers are typically grown before the heterolayers under study. These may be thick buffer layers or short-period superlattices.

The development of MBE technology has stimulated intense experimental and theoretical research on exciton states in quantum wells (QWs); see, e.g., Refs. [5,20–29]. Exciton states and exciton-light coupling in various heterostructures are now well understood. The recently developed microscopic modeling of exciton states in QWs [13–15] allows one to quantitatively analyze reflectance spectra and to obtain valuable information about exciton states in heterostructures studied experimentally. The parameters of the exciton states obtained in such an analysis are unambiguously related to structural characteristics of the samples studied. This provides a theoretical basis for using excitons as a probe for a quantitative study of the design and quality of real structures.

We have already used an excitonic probe to study the spin dynamics of nonradiative excitons in a QW [30]. In the present paper, we apply an excitonic probe to analyze

*philipp0grigoriev@gmail.com

 © 2019 American Physical Society

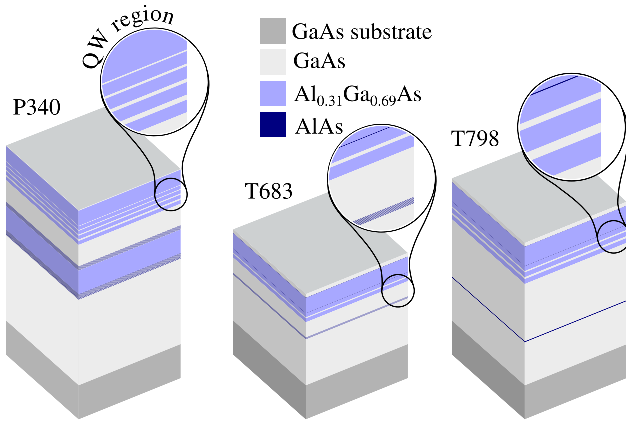

FIG. 1. Heterostructures studied in the present work.

the peculiarities of the MBE process, which is vital for the growth of high-quality structures. Using an example of three significantly different heterostructures (see Fig. 1), we demonstrate the universal capabilities of the exciton-probe method. In particular, we focus on the criteria of high optical quality and discuss technological methods that are promising for obtaining further increase of that quality.

Optical examination, such as the use of reflectance spectroscopy, can detect only faults with sizes comparable to the wavelength of light. Light, however, can create an exciton with a wave function whose effective size is as small as the diameter of the exciton (30 nm for GaAs). These excitons, therefore, can detect tiny imperfections with a size corresponding to that of the wave function. Only a photon is needed to create an exciton probe, which makes excitons a simple, yet powerful, tool for the examination of nanostructures.

Here we consider three cases of the use of excitons as a probe in the examination of planar heterostructures. The structures are grown by MBE technology on 2-inch GaAs substrates with a (001) orientation. When needed, substrates are rotated during growth to reduce gradients in the epitaxial layers. For this study, we have selected the highest-quality structures. The optical characterization is performed by focusing the incident light into a small spot with a diameter of about 50 μm on selected positions on the sample surface.

The paper is organized as follows. Exploiting a standard theoretical model, we discuss a general case of narrow QWs in Sec. III. Then we present the case of a sample designed to simplify the data treatment. Finally, we apply our approach to wide QWs with multiple exciton resonances in Sec. V. A conclusion section completes our study.

II. STANDARD MODEL

The standard model was first developed for the ground states of excitons in narrow QWs (see Refs. [31–36] and the textbook by Ivchenko [24]). Later it was generalized to wider QWs with multiple but distinct exciton transitions [12]. The generalization also works well for asymmetric QWs [14].

This model reduces the reflectance of a heterostructure to the reflectance of multiple spatially separated surfaces. Amplitude reflection coefficients are assigned to each surface. For normal incidence, the amplitude reflectance of the sample surface is

$$r_s(\omega) = \frac{n_{\rm out} - n_{\rm in}(\omega)}{n_{\rm out} + n_{\rm in}(\omega)}, \tag{1}$$

where $n_{\rm out} = 1$ in our case. For the GaAs capping layer, $n_{\rm in}(\omega) \approx 3.6$ near the band-gap photon energy, and $r_s(\omega)$ is negative, as for any dielectric surface. As shown in Ref. [24], a QW with an exciton resonance reflects light like a surface at the center of the QW layer, with an amplitude reflection coefficient

$$r_X(\omega) = \frac{i\Gamma_0}{(\tilde{\omega}_0 - \omega) - i(\Gamma_0 + \Gamma)}. \tag{2}$$

Here $\tilde{\omega}_0 = \omega_0 + \delta\omega_0$ is the resonance frequency, where ω_0 is the frequency of a mechanical exciton and $\delta\omega_0$ is the frequency shift induced by the exciton-light coupling [15,24]. The quantity Γ_0 describes the decay of the exciton through the radiative channel and Γ accounts for all nonradiative losses of the exciton, including the loss of exciton coherency. These are the radiative and nonradiative decay rates, respectively.

The intensity reflection coefficient can be obtained by the use of a standard transfer matrix formalism [24]:

$$R_m(\omega) = \left| \frac{r_s(\omega) + \sum_j^m r_{Xj}(\omega) e^{i2\phi_j}}{1 + r_s(\omega) \sum_j^m r_{Xj}(\omega) e^{i2\phi_j}} \right|^2, \tag{3}$$

where ϕ is the phase shift acquired by the light propagating from the sample surface to the middle of the QW. Equation (3) assumes a sufficient energy separation of the exciton resonances. Otherwise, the exciton-light-induced coupling of exciton states should be taken into account [15,37]. In Eq. (3), we also neglect for simplicity a nonresonant reflection from the QW interfaces. It can be taken into account as described in Ref. [38].

To quantify the standard model, we calculate the main exciton parameters, namely, the exciton transition energy $\hbar\omega_0$ and the radiative broadening $\hbar\Gamma_0$, by numerical solution of the three-dimensional Schrödinger equation for an exciton in a QW, as described in Ref. [13]. Our approach provides a solid foundation for the standard model. Without theoretical simulation, this model is just a large set of unknown exciton parameters defining the resonant reflectance response.

III. STRUCTURES WITH MULTIPLE NARROW QWS

First we demonstrate how our approach can be used to determine the design of an actual heterostructure. A structure, P340, containing four narrow QWs is studied. A summary of the structure describing all layers is given in Table I. The structure contains many technological layers that prevent dislocations in the substrate growing through the epitaxial layers. The technological parameters for each layer are adjusted during growth.

We calculate the expected reflectance spectrum for the heterostructure grown; see Fig. 2. The exciton wave functions are obtained by numerical solution of the Schrödinger equation for an exciton in the QW with the material parameters given in Refs. [13,39]. The eigenvalue obtained from the solution is the exciton energy $\hbar\omega_0$. We neglect for simplicity the energy shift $\hbar\delta\omega_0$ because it is small for narrow QWs [15]. The radiative constant is calculated as [13,14,24]

$$\hbar\Gamma_0 = \frac{1}{2} q \hbar\omega_{\rm LT} \pi a_B^3 \left| \int \Phi(z) e^{iqz} dz \right|^2, \qquad (4)$$

where q is the wave vector of the light, $\hbar\omega_{\rm LT}$ is the longitudinal-transverse splitting, a_B is the exciton Bohr radius in the bulk GaAs, and $\Phi(z)$ is the cross section of the exciton wave function along the growth axis z for coinciding electron and hole coordinates. The exciton energy determines the energy position of the exciton resonance, and the radiative constant determines its amplitude; see Eqs. (2) and (3).

The exciton resonance profile is controlled also by the phase shift and the nonradiative constant. On passing through a layer of thickness L with refractive index n, the light acquires a phase shift $\phi = k_0 L n$, where $k_0 = 2\pi/\lambda$ is the wave vector of the light in vacuum. The quantity $L^o = Ln$ is the so-called optical length. For a heterostructure with many layers, the phase shift is

$$\phi = k_0 L^o \times k_0 \sum_j L_j n_j + \frac{L_{\rm QW} n_{\rm QW}}{2}. \qquad (5)$$

TABLE I. Structural parameters of sample P340.

Function	Content	Thickness (nm)
Substrate	GaAs (100)	
Technological		
Buffer	GaAs	1116
Superlattice	3 × ((Al,Ga)As + GaAs)	24.4
Superlattice	11 × ((Al,Ga)As + GaAs)	52.8
Barrier	$Al_{0.31}Ga_{0.69}As$	314
Superlattice	11 × (GaAs + AlAs)	55
Buffer	GaAs	282.7
Heterostructure		
Barrier	$Al_{0.34}Ga_{0.66}As$	49.5
QW	**GaAs**	**19.8**
Barrier	$Al_{0.34}Ga_{0.66}As$	49.5
QW	**GaAs**	**14.0**
Barrier	$Al_{0.34}Ga_{0.66}As$	49.5
QW	**GaAs**	**9.3**
Barrier	$Al_{0.34}Ga_{0.66}As$	49.5
QW	**GaAs**	**5.6**
Barrier	$Al_{0.34}Ga_{0.66}As$	198.1
Cap layer	GaAs	9.3

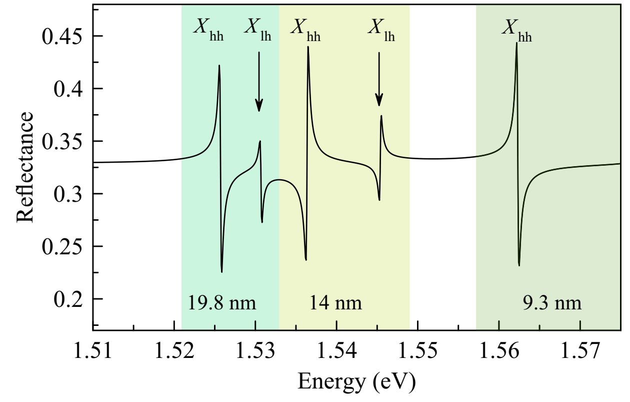

FIG. 2. Expected reflectance spectrum for structure P340. The spectrum is calculated from a microscopic solution of the Schrödinger equation for an exciton in a QW.

The refractive indices of the GaAs and (Al, Ga)As layers depend noticeably on the photon energy in the spectral range of the exciton resonances under discussion. We approximate these dependencies by a phenomenological function,

$$n(E) = n_0(E_g) + b(E - E_g) + a(E - E_g)^2, \qquad (6)$$

with the parameters given in Table II and $E_g = 1.519$ eV. The phase shifts calculated with the use of Eqs. (5) and (6) and the layer thicknesses listed in Table I predict dispersionlike profiles of the exciton resonances; see Fig. 2.

The nonradiative broadening of exciton resonances, $\hbar\Gamma$, cannot be theoretically calculated. In high-quality heterostructures, it is mainly controlled by the collisions of excitons with other quasiparticles such as phonons, free carriers, and nonradiative excitons [30,41]. In the calculations of spectra shown in Fig. 2, we take $\hbar\Gamma = 100$ μeV, a value that is typical of high-quality heterostructures [12,14,30].

TABLE II. Refractive-index parameters for Eq. (6) [5,40].

	n_0	$b\,({\rm eV}^{-1})$	$a\,({\rm eV}^{-2})$
GaAs	3.6057	0.7601	1.2176
$Al_{0.34}Ga_{0.66}As$	3.3474	0.3574	0.1693

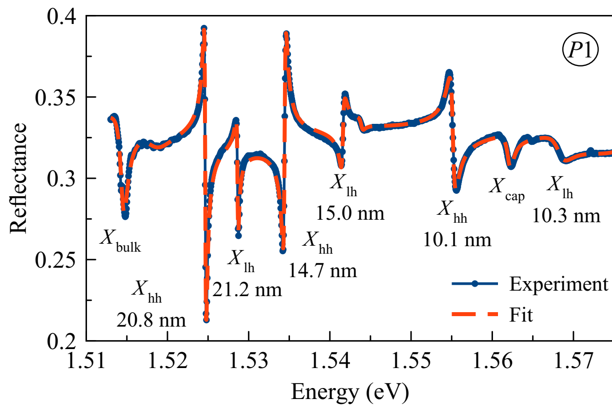

FIG. 3. Reflectance spectrum of structure P340 measured at point $P1$ (blue curve). Exciton resonances for three GaAs/Al_xGa_{1-x}As QWs with nominal thicknesses $L = 19.8$ nm, 14 nm, and 9.3 nm are clearly seen. The red curve is a fit obtained with the standard model. The labels X_{hh} and X_{lh} mark the heavy-hole and light-hole exciton resonances, respectively, X_{bulk} is the exciton resonance in the GaAs buffer layer, and X_{cap} is presumably the exciton resonance in the cap layer. The QW widths obtained from the energy positions of the resonances are given near each resonance. Sample temperature $T = 10$ K.

The experimentally obtained reflectance spectrum of sample P340 is shown in Fig. 3 for a point $P1$ on the sample. This point is close to the point where the growth rate is measured during the MBE process using a reflection high-energy electron diffraction (RHEED) method. The spectrum displays several exciton resonances for the QWs under study, marked X_{hh} and X_{lh}. There are also resonances at higher energies beyond the spectral range shown in Fig. 3, which can be attributed to an exciton transition in the 5-nm QW. These resonances are considerably broadened, and we do not discuss them in the present paper. We also do not discuss resonances related to exciton transitions in the GaAs buffer layers and the thin capping layer.

Comparison of Figs. 2 and 3 shows a close similarity of the experimental and theoretical spectra. In particular, both the energy positions and the profiles of the exciton resonances are well reproduced in the model. Hence, the relatively simple expressions (1)–(6) take into account all important characteristics of the heterostructure and the exciton-light coupling.

Nevertheless, there is a quantitative difference between these spectra, which provides a deeper insight into the properties of the structure grown. To quantify these differences, we fit the experimental spectrum by Eqs. (2) and (3), considering all four parameters ω_{0j}, Γ_{0j}, Γ_j, and ϕ_j for each exciton resonance as fitting parameters. Figure 3 shows that the fitted curve almost perfectly reproduces the experimental spectrum; therefore, the values of the fitting parameters are obtained with good accuracy. They are listed in Table III.

Here we discuss only the energies and phases of the exciton resonances. The radiative broadening as a function of the QW width is extensively discussed in Ref. [13]. The nonradiative broadening is a phenomenological parameter. For the structure under study, it is larger than the value for the best-quality structures [12,30]. At the same time, it is small enough to allow one to reliably determine the exciton energies and the phase shifts.

First we discuss the energies of the exciton transitions, $E_X = \hbar\omega_0$. The fitting with the standard model gives the energies E_X with an accuracy of several tens of μeV. On the other hand, the energy of an exciton in a QW can be calculated numerically with high precision. By solving a Schrödinger equation (see Ref. [13] for details), we obtain the exciton energy as a function of the QW width [42]. The material parameters used were the same as in Ref. [13].

Figure 4 shows the exciton energies obtained from the fitting of the experimental data, and the dependencies obtained numerically. As can be seen from the figure, the experimentally obtained energies (open circles) are close to the theoretical curves. There is, however, a systematic deviation towards smaller QW widths. We assume that the structure grown has a gradient in the layer thicknesses. Such a gradient is typically present in MBE-grown structures when the substrate is not rotated during growth [17]. This is the case for our sample. A comparison of the energies obtained from the experiment and from the modeling

TABLE III. Exciton parameters for structure P340.

	L_{QW}	Type	E_X (eV)	$\hbar\Gamma_0/\hbar\Gamma$ (μeV)	$2\phi_{exp}$	$2\phi_{calc}$
$P1$	19.8 nm	hh	1.52467	22/110	1.95	$1.96 + 6\pi$
		lh	1.52864	11/110	2.04	$2.03 + 6\pi$
	14 nm	hh	1.53444	31/150	−1.68	$-1.48 + 6\pi$
		lh	1.54160	13/225	−1.76	$-1.42 + 6\pi$
	9.3 nm	hh	1.55513	33/340	1.67	$1.75 + 4\pi$
		lh	1.56835	21/1150	2.09	$1.89 + 4\pi$
$P2$	19.8 nm	hh	1.53109	28/250	−1.54	$-1.64 + 6\pi$
		lh	1.53832	18/400	−1.60	$-1.55 + 6\pi$
	14 nm	hh	1.54470	38/400	1.80	$1.86+4\pi$

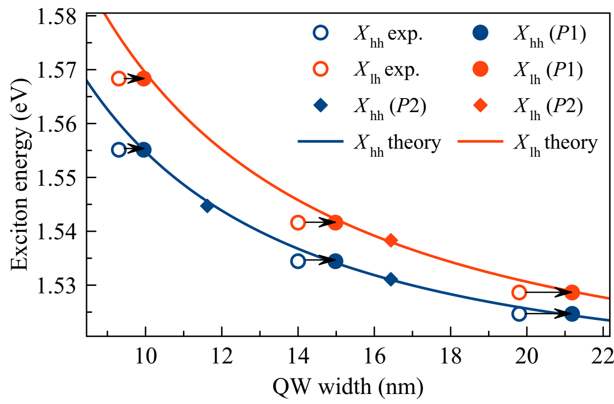

FIG. 4. Heavy-hole (blue) and light-hole (red) exciton energies vs QW width. The solid lines show microscopic calculations of the exciton energies. The open symbols correspond to the measured exciton energies assuming the nominal widths of the QWs. The filled symbols show the exciton energies in QWs with the real widths, calculated as $1.07L_j$ for point $P1$ and $0.83L_j$ for point $P2$ (see text for details). The arrows show the shift of the experimental data when the nominal width is replaced by the real QW width.

allows us to determine the real QW widths at the point $P1$ studied. They are given in Fig. 3. On average, the real widths are larger by a factor of $K_{\mathrm{QW}} = 1.07$ than the nominal widths given in Table I. By multiplying the QW widths by this factor, we can move the experimental data almost exactly onto the theoretical curves; see the filled circles in Fig. 4.

The presence of a gradient in this structure is easily verified by studying a reflectance spectrum at another point on the sample. An example of a spectrum measured at a point $P2$ is shown in Fig. 5. This point is at a distance of 10 mm from point $P1$ along the direction of the maximum gradient of the GaAs layer thickness in the structure grown. As can be seen from the figure, the observed resonances for the nominally 19.8-nm and 14-nm QWs are blueshifted relative to those observed at point $P1$. This fact means that the real QW widths at point $P2$ are considerably smaller than the nominal widths. By multiplying the nominal QW widths by a factor of $K_{\mathrm{QW}} = 0.83$, we again obtain good correspondence with the theoretical calculations; see the diamond symbols in Fig. 4. The exciton energies obtained for points $P1$ and $P2$ allow us to estimate the gradient of the QW width, $(1/L)(dL/dx) \approx 0.024\ \mathrm{mm}^{-1}$. This is determined by the gradient of the growth rate of the GaAs layers, which is mainly governed by the gradient of the Ga BEP.

Let us now discuss the phases of the exciton resonances, which determine their profile. The phases are very sensitive to the total optical thickness of the layers through which the light propagates to the QW containing the exciton. The phases obtained experimentally can be compared with those calculated from Eq. (5). The gradient for the

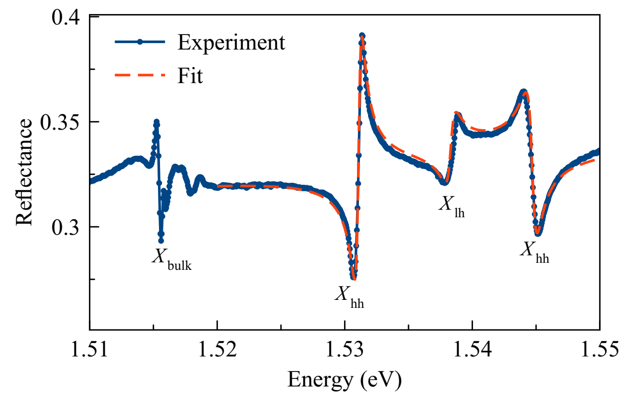

FIG. 5. Reflectance spectrum of structure P340 measured at point $P2$ (blue curve). The red dashed curve is a fit by Eqs. (2) and (3). A strong blueshift of all exciton resonances is clearly seen (compare with Fig. 3). Sample temperature $T = 10$ K.

$\mathrm{Al}_x\mathrm{Ga}_{1-x}\mathrm{As}$ barrier layers may differ from that for the GaAs QW layers. Besides, the aluminum content x may also vary from point to point on the sample, which changes the height of the barrier and its refractive index. To simplify the problem, we use only one free parameter, K_b, scaling the optical thickness of the barrier layers. The best correspondence of the calculated phases with those obtained from the experiment is achieved when $K_b = 1.00$ for point $P1$ and $K_b = 0.83$ for point $P2$. The results are given in Table III. The calculated phase in this table is presented as a sum, $2\phi_{\mathrm{calc}} = 2\,\Delta\phi_{\mathrm{calc}} + m2\pi$, because the experiment gives the value of the phase only up to a natural-number multiple of 2π.

A visual illustration of the phase shifts is shown in Fig. 6. The green areas show the optical thicknesses of the QWs, $L_{\mathrm{QW}}n_{\mathrm{QW}}$, whose positions are determined by the total optical thickness of all preceding layers from the

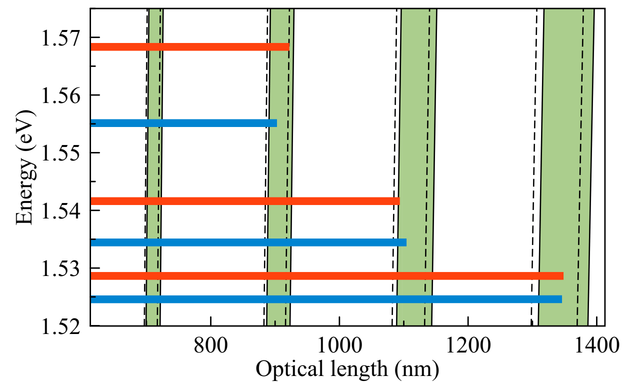

FIG. 6. Optical lengths restored from the phases ϕ_{exp} for point $P1$. The dashed lines show the nominal positions of the QW interfaces. The green areas show the real QW layer positions. The blue bars correspond to the optical length for the X_{hh} excitons and the red bars correspond to that for the X_{lh} excitons.

top of the sample. The nominal positions of the QWs are shown by the dashed lines. The nominal and real positions depend on the photon energy via the refractive index. The horizontal stripes show the experimentally obtained optical path for each exciton resonance, $L_X^o = (\phi_{\rm exp} + m\pi)/k_0$, where $m = 2$ for the 9.3-nm QW and $m = 3$ for the 14-nm and 19.8-nm QWs.

Figure 6, while consistent in general, gives a sense of the accuracy of the phase determination. In fact, the optical lengths for heavy-hole and light-hole excitons created in the same QW should coincide up to the refractive-index dependence (6). As one can see in Fig. 6, this relation is not exactly fulfilled.

Finally, we would like to emphasize that the phase is sensitive to small changes in the layer thickness. For example, a change in the thickness of 2 nm gives rise to a 0.1-radian phase change, which is easily observable in high-quality structures. This sensitivity, together with precise experimental determination of the exciton energies, can be used for further verification of the theoretical model and the structural parameters.

IV. 0 AND π PHASE CASES

Phase control paves the way to designing heterostructures with easily interpreted reflectance spectra. In the case of a phase $2\phi = 0$, the exciton resonance reveals itself in the spectrum as a peak. This is simply due to constructive interference of the light waves reflected from the sample surface and from the QW. In the case of a phase $2\phi = \pm\pi$, the interference is destructive and the exciton resonance is shown by a dip.

Figure 7 shows a reflectance spectrum of a structure, T798, with 20-nm and 14-nm QWs. The design of this structure is presented in Table IV. A thin AlAs layer in the technological part of the structure prevents dislocations in the layers under study. The barrier layers contain a small aluminum fraction of 2.8%, which is found to improve the quality of the structure. Thin AlAs insets in the top barrier layer are grown to increase the PL yield from the layer; this is not discussed in this paper.

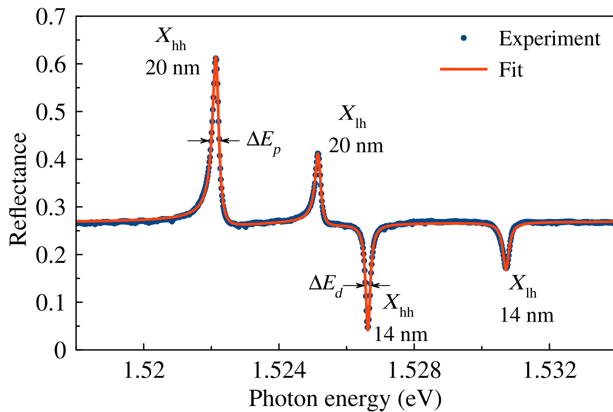

FIG. 7. Reflectance spectrum of sample T798 with 20-nm and 14-nm $GaAs/Al_{0.028}Ga_{0.972}As$ QWs (solid line). The dashed line shows fits by Eqs. (2) and (3). The labels $X_{\rm hh}$ and $X_{\rm lh}$ mark the heavy-hole and light-hole exciton resonances, respectively. Sample temperature $T = 10$ K.

TABLE IV. Structural parameters of sample T798.

Function	Content	Thickness (nm)
Substrate	GaAs (100)	
Techn.		
Buffer	GaAs	450
Barrier	AlAs	10
Thick buffer	GaAs	600
Heterostructure		
Barrier	$Al_{0.031}Ga_{0.969}As$	50
QW	**GaAs**	**20**
Barrier	$Al_{0.031}Ga_{0.969}As$	50
QW	**GaAs**	**14**
Barrier	$Al_{0.031}Ga_{0.969}As$	50
Barrier	AlAs	2.5
Barrier	$Al_{0.031}Ga_{0.969}As$	200
Barrier	AlAs	2.5
Cap layer	GaAs	40

Because of the special design of this structure, namely, an appropriate choice of thickness of the barrier layers, the exciton resonances reveal themselves as peaks or dips. We attribute the peaks to exciton transitions in the 20-nm QW and the dips to exciton transitions in the 14-nm QW. The small spectral width of the resonances and their Lorentzlike shape indicate the high quality of this structure.

The exciton resonances are well fitted by the standard model, Eqs. (2) and (3). The fitting parameters are listed in Table V. The nonradiative broadening of the resonances does not exceed 0.1 meV. In particular, it is close to the radiative broadening of the $X_{\rm hh}$ exciton in the 20-nm QW. The phases of the peaklike exciton resonances are relatively small. For the dips, they are close to $-\pi$.

The full width at half maximum (FWHM) of the resonances, denoted by ΔE in Fig. 7, differs for peaks and dips. In particular, ΔE for the $X_{\rm hh}$ peak for the 20-nm QW is larger than that for the $X_{\rm hh}$ dip for the 14-nm QW, although the sums of the radiative and nonradiative broadenings

TABLE V. Exciton parameters for structure T798.

$L_{\rm QW}$ (nm)	Type	E_X (eV)	$\hbar\Gamma_0$ (μeV)	$\hbar\Gamma$ (μeV)	$2\phi_{\rm exp}$ (rad)
20 nm	hh	1.52214	42	50	0.34
	lh	1.52516	18	74	0.42
14 nm	hh	1.52663	35	66	−3.10
	lh	1.53071	16	100	−3.13

of these resonances are almost equal; see Table V. The origin of this difference is the background reflection from the sample surface. The reflectance at the peak is described by

$$R_p = \left| \frac{(\Gamma_0 + \Gamma) r_s - \Gamma_0}{(\Gamma_0 + \Gamma) - r_s \Gamma_0} \right|^2 . \qquad (7)$$

This expression follows from Eqs. (2) and (3) assuming $\omega = \tilde{\omega}_0$ and $\phi = 0$. Introducing variables

$$\begin{aligned} A &= [(\Gamma_0 + \Gamma) r_s - \Gamma_0], \\ B &= [(\Gamma_0 + \Gamma) - r_s \Gamma_0], \end{aligned} \qquad (8)$$

we can write an equation for the half-maximum frequency, $\delta\omega_p$,

$$\left| \frac{\delta\omega_p r_s - iA}{\delta\omega_p - iB} \right|^2 = r_s^2 + \frac{1}{2} \left(\frac{A^2}{B^2} - r_s^2 \right). \qquad (9)$$

Here r_s^2 is the background reflection and $(A^2/B^2 - r_s^2)$ is the peak amplitude. It is easy to see that this equation is satisfied when $\delta\omega_p = B$.

Owing to the negative r_s, the FWHM of a peaklike exciton resonance is

$$\Delta E_p = 2\hbar [(\Gamma_0 + \Gamma) + |r_s| \Gamma_0], \qquad (10)$$

which is larger than the sum of the radiative and nonradiative broadenings, $2\hbar(\Gamma_0 + \Gamma)$.

In the case of a diplike resonance, the phase ϕ is equal to $\pi/2$ and the reflectance at the dip is described by

$$R_d = \left| \frac{(\Gamma_0 + \Gamma) r_s + \Gamma_0}{(\Gamma_0 + \Gamma) + r_s \Gamma_0} \right|^2 . \qquad (11)$$

This expression resembles Eq. (7) within a sign. Similar mathematical transformations give rise to the final expression for the FWHM of the dip,

$$\Delta E_d = 2\hbar [(\Gamma_0 + \Gamma) - |r_s| \Gamma_0]. \qquad (12)$$

This value is obviously smaller than the sum $2\hbar(\Gamma_0 + \Gamma)$. For the resonances shown in Fig. 7, we obtain $\Delta E_p = 227$ μeV and $\Delta E_d = 141$ μeV. Here we use the value $|r_s| = 0.516$ obtained from the fit of the experimental spectrum. So, the ratio $\Delta E_p / \Delta E_d = 1.6$ is mainly related to the background reflection from the surface of the structure.

The peaklike or diplike exciton resonances in the reflectance spectra of specially designed heterostructures can be fitted by Lorentzians if the inhomogeneous broadening is negligible. The exciton parameters can be recovered from the Lorentz FWHM with Eqs. (10) and (12). This further simplifies the processing of the experimental data.

The standard model can also be reduced to Lorentzian fittings if one measures the reflectance at the Brewster angle [11]. This approach is discussed in the next section.

V. HETEROSTRUCTURES WITH WIDE QUANTUM WELLS

The reflectance spectra of wide QWs show multiple resonances if the quality of the heterostructure is high enough [15,43–45]. These resonances correspond to optical transitions to excited quantum-confined exciton states. The exciton-light coupling increases with the QW width, so that the high-energy states become clearly visible. Simultaneously, the energy separation between neighboring states decreases, and several low-lying states are mixed by light and cannot be separated [15,37].

Reflectance spectra at the Brewster angle provide exciton resonances in the form of Lorentz peaks independent of the design of the structure [11]. This simplification, however, comes with several drawbacks. First, the Brewster angle can only be achieved for a single wavelength, due to the dependence of the refractive index on the photon energy. Second, the inclined light beam can, in principle, excite so-called longitudinal excitons [24]. These are excitons propagating in the QW plane with the vector of the exciton polarization perpendicular to the plane. Finally, a significant beam inclination decreases the exciton-light coupling by a factor of $\cos\theta$, where θ is the inclination angle inside the structure.

However, longitudinal heavy-hole excitons are absent in GaAs QWs. In addition, due to the high refractive index of GaAs, the internal inclination angle θ is approximately equal to 15°, which follows from Snell's law, $\sin\theta = \sin\theta_{\text{ext}}/n(\text{GaAs})$, where θ_{ext} is the external incidence angle. Therefore the difference in reflectance spectra measured at the Brewster angle and at normal incidence is not so dramatic.

Figure 8 shows a reflectance spectrum of a heterostructure with a 200-nm GaAs/(Al, Ga)As QW measured at the Brewster angle [46]. Despite the fine tuning of the incidence angle of the light, we still observe a small background reflectance of nearly 0.5%. It grows with the photon energy, so that the high-energy exciton resonances are revealed as peaks and dips. The peaks are the even exciton states, while the dips are the odd states, as verified by the microscopic modeling described below. Note that the exciton-light coupling constants for the even and odd exciton states in the 200-nm QW are comparable [15].

We associate the presence of many clearly visible high-energy exciton resonances with the high quality of the QW interfaces. The exciton-light coupling for the high-energy states is largely determined by the near-interface layers, with a thickness of about the exciton Bohr radius, as a theoretical analysis in Ref. [15] shows. This makes the

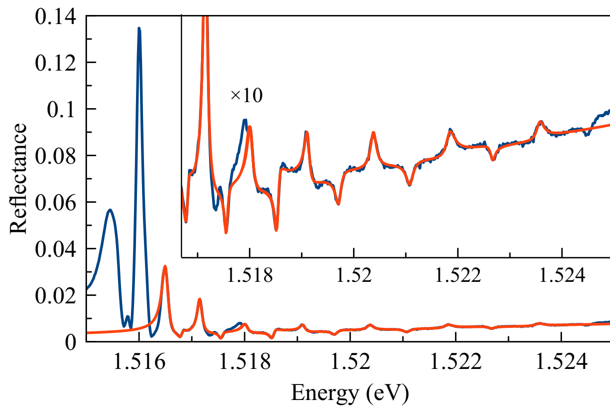

FIG. 8. Reflectance spectrum of structure T683 with a 200-nm GaAs/(Al, Ga)As QW measured at the Brewster angle, $\theta_{\text{ext}} = \theta_B \approx 75^\circ$. The red line shows a fit by Eqs. (2) and (3).

high-energy exciton resonances a very sensitive tool for probing the interface quality.

In the heterostructure under study, two different technological methods are used to increase the interface quality. The bottom QW barrier is grown as a short-period superlattice; see Table VI. This allows us to eliminate the influence of dislocations on the quality of the crystal structure. Besides, short growth interruption intervals of 1 s are used after the growth of each superlattice layer. This interruption provokes migration of atoms on the surface, thus smoothing the interface before growing the QW layer.

The growth of the top QW interface is preceded by a long interruption time of 60 s to smooth the interface. This time interval is chosen according to the restoration dynamics of the RHEED pattern. This pattern is observed with blocked gallium and aluminum beams and an opened As beam. We should emphasize that the growth interruptions require a high-vacuum environment, which is achieved in our case by a combination of turbomolecular, ion, and cryogenic vacuum pumps.

TABLE VI. Structural parameters of sample T683.

Function	Content	Thickness (nm)
Substrate	GaAs (100)	
Techn.		
Buffer	GaAs	600
Superlattice	$10 \times (\text{AlAs} + \text{GaAs})$	26.5
Heterostructure		
QW	**GaAs**	**200**
Barrier	$Al_{0.035}Ga_{0.965}As$	50
QW	**GaAs**	**14**
Barrier	$Al_{0.035}Ga_{0.965}As$	50
Barrier	AlAs	3
Barrier	$Al_{0.035}Ga_{0.965}As$	200
Barrier	AlAs	3
Cap layer	GaAs	50

The standard model described above can be easily modified for the case of an inclined incident light beam [24]. Equation (2) for the amplitude reflectance of the isolated exciton resonance requires a replacement of Γ_0 by $\Gamma_0 \cos\theta$ and an additional frequency shift,

$$r_X(\omega) = \frac{i\Gamma_0 \cos\theta}{(\tilde{\omega}_0 + \delta\omega_{\text{kin}} - \omega) - i(\Gamma_0 \cos\theta + \Gamma)}. \quad (13)$$

The frequency shift, $\delta\omega_{\text{kin}} = \hbar q_x^2/(2M)$, is due to exciton propagation in the QW plane. Here M is the exciton mass and q_x is the in-plane component of the exciton wave vector. Because of momentum conservation, q_x coincides with the in-plane wave vector of the light. In Eq. (13), we ignore longitudinal excitons and also consider only p-polarized incident light. A full treatment can be found in Ref. [24].

Equation (3) must also be modified to take into account the incidence angle:

$$R_m(\omega) = \left| \frac{r_s(\theta_{\text{ext}}, \omega) + \sum_j^m r_{Xj}(\omega) e^{i2\phi_{\theta j}}}{1 + r_s(\theta_{\text{ext}}, \omega) \sum_j^m r_{Xj}(\omega) e^{i2\phi_{\theta j}}} \right|^2. \quad (14)$$

The phase shift ϕ_θ for the incidence of light on the sample surface at the angle θ_{ext} is easy to express in terms of the phase shift ϕ_0 for normal incidence: $\phi_\theta = \phi_0 \cos\theta$, which is the thin-film-interference phase delay.

Although Eqs. (13) and (14) differ from Eqs. (2) and (3), this difference does not affect the accuracy of the phenomenological fit. Obviously, the sets of fitting parameters in the two pairs of the equations are equivalent. In the fitting of the experimental spectrum shown in Fig. 8, a linear approximation for the frequency dependence of $r_s(\theta_{\text{ext}}, \omega)$ in the energy range 1.516–1.523 eV is used. The low-lying exciton resonances are not fitted, because of their strong light-induced mixing [15,37]. We also ignore some peculiarities in the spectrum, assuming that they are related to the light-hole excitons.

To analyze the low-energy part of Fig. 8 and, in particular, to attribute the observed resonances to particular exciton states, we find wave functions numerically for the heavy-hole exciton in a 200-nm QW and recover the spectrum using Eqs. (13) and (14). Furthermore, we take the light-induced coupling of the exciton states into account. The details of the numerical procedure are described in Ref. [15].

Figure 9 compares the experimental data with the results obtained numerically. There is overall agreement between the experimental and theoretical spectra. As seen, consideration of the light-induced coupling of the exciton states improves the agreement. However, some details of the experimental spectrum are not reproduced in the modeling. We assume that this is due to contributions from the light-hole excitons. In fact, the ground states of the X_{hh} and X_{lh} excitons are almost degenerate in a wide QW

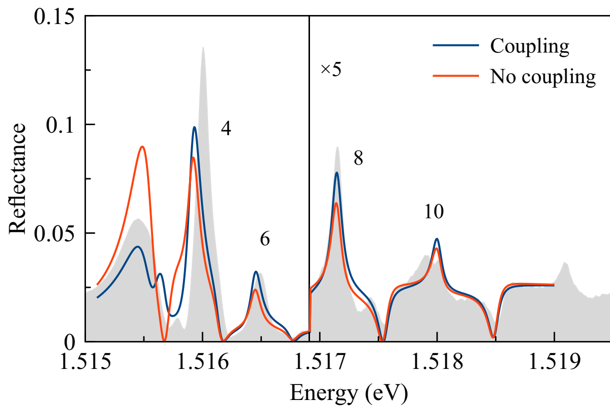

FIG. 9. Microscopic modeling of the reflectance spectrum measured at the Brewster angle for structure T683 with a 200-nm GaAs/(Al, Ga)As QW. The blue curve shows the spectrum calculated with allowance for the light-induced coupling of exciton states (model by Voronov *et al*. [37]). The red curve is obtained from a simplified calculation with no coupling. The experimental spectrum is shown by the gray shaded area. The numbers indicate the even quantum-confined exciton states.

and, as a result, the electron-hole Coulomb interaction couples them efficiently. Modeling of the coupled exciton states requires a numerical solution of a four-dimensional Schrödinger equation, which includes a 4×4 Luttinger Hamiltonian [47]. Such a complex problem has not been solved yet.

Nevertheless, the microscopic modeling allows one to identify separate exciton resonances and to describe their profiles reasonably well for photon energies $E > 1.516$ eV. This somewhat unexpected good agreement between the experiment and the theory may possibly be explained by the exciton-light coupling constant for the light-hole exciton being three times smaller than that for the heavy-hole exciton. Besides, the spectrum of the X_{lh} exciton states is sparse relative to that of the X_{hh} excitons due to the smaller effective mass.

VI. CONCLUDING REMARKS

In this paper, we demonstrate that an excitonic probe is an efficient tool to quantitatively study both the parameters and the structural quality of a heterostructure. Reflectance spectroscopy allows one to obtain a full set of all four parameters for each exciton resonance. Numerical solution of the three-dimensional Schrödinger equation provides the exciton energies $\hbar\omega_{0j}$ and the exciton-light coupling constants $\hbar\Gamma_{0j}$ with no approximations. The model relies on the material parameters, which are published in the literature. So, a comparison of the experimental exciton energies with the results of modeling is sufficient to extract the thickness of the QW layers.

The constants $\hbar\Gamma_{0j}$ are useful for determining the quality of a structure. In particular, the quality is high when the radiative broadening is a significant part of the total broadening of the exciton resonances. The radiative constants for the high-energy exciton states in wide QWs characterize the quality of the QW interfaces. When the quality is not high enough, the experimentally obtained constants become smaller than the theoretical values, and the excited exciton states become invisible in low-quality structures.

The phase shifts of the exciton resonances, ϕ_j, contain valuable information about the layer thicknesses. Several examples discussed in this paper clearly show that the total thickness of the layers from the sample surface to the QW under study may be obtained with an accuracy of a few nanometers.

The last parameter of an exciton resonance is the nonradiative broadening $\hbar\Gamma_j$. This is governed by the quality of the heterostructure. The nonradiative broadening, in general, consists of homogeneous and inhomogeneous contributions [48]. The latter arises when the exciton "feels" a static fluctuating potential in the heterostructure. The presence of this broadening is a clear sign of low quality of the heterostructure. If the statistics of the fluctuations is Gaussian, the wings of the exciton resonances decay faster with energy (Gaussianlike wings) than in the case of homogeneous broadening (Lorentzianlike wings). This difference, in principle, allows one to separate the homogeneous and inhomogeneous contributions. Equations (2) and (3) do not include effects related to inhomogeneity of the exciton ensemble. Therefore they are applicable only in the case of high-quality heterostructures, in which the inhomogeneous exciton line broadening is negligible.

The homogeneous broadening may, in turn, consist of several contributions, some of which are of fundamental nature. These are the exciton-exciton, exciton-phonon, and exciton-carrier interactions extensively discussed in the literature. An experimental study of this broadening contains information about the dynamics of interacting systems [11,12,30,41]. This broadening can be minimized by an appropriate choice of experimental conditions. These conditions may be the use of a low sample temperature (suppression of exciton-phonon interactions), resonant and nonperturbative optical excitation (suppression of free-carrier generation), etc. For high-quality heterostructures, the broadening can be minimized down to the radiative broadening. On the other hand, in low-quality heterostructures, homogeneous broadening can be caused by strong nonradiative channels for exciton disappearance due to electron-hole relaxation via deep centers. In this case, the broadening remains large under all experimental conditions.

In summary, the exciton parameters allow one to determine the layer thicknesses in a QW and the thicknesses of the barrier layers. An excitonic probe is, therefore, an excellent tool for the characterization of epitaxial heterostructures, providing full information on structural parameters as well as on crystal-structure quality.

ACKNOWLEDGMENTS

The authors thank V. S. Zapasskii for fruitful discussions of this paper and the SPbU Resource Center "Nanophotonics" [49] for the heterostructures studied in this work. Financial support from the Russian Science Foundation, Grant No. 19-72-20039, is acknowledged.

[1] *Molecular Beam Epitaxy: From Research to Mass Production*, edited by Mohamed Henini (Elsevier Inc., Amsterdam, 2013).

[2] J. Faist, *Quantum Cascade Lasers* (Oxford University, Oxford, 2013).

[3] Q. Lu and M. Razeghi, Recent advances in room temperature, high-power terahertz quantum cascade laser sources based on difference-frequency generation (review), Photonics **3**, 42 (2016).

[4] M. Piccardo, P. Chevalier, T. S. Mansuripur, D. Kazakov, Y. Wang, N. A. Rubin, L. Meadowcroft, A. Belyanin, and F. Capasso, The harmonic state of quantum cascade lasers: Origin, control, and prospective applications [Invited], Opt. Express **26**, 9464 (2018).

[5] A. V. Kavokin, J. J. Baumberg, G. Malpuech, and F. P. Laussy, *Microcavities* (Oxford University Press, Oxford, 2017), 2nd ed.

[6] L. H. Li, J. X. Zhu, L. Chen, A. G. Davies, and E. H. Linfield, The MBE growth and optimization of high performance terahertz frequency quantum cascade lasers, Opt. Express **23**, 2720 (2015).

[7] Y. Sun, P. Wen, Y. Yoon, G. Liu, M. Steger, L. N. Pfeiffer, K. West, D. W. Snoke, and K. A. Nelson, Bose-Einstein Condensation of Long-Lifetime Polaritons in Thermal Equilibrium, Phys. Rev. Lett. **118**, 016602 (2017); Erratum: [Phys. Rev. Lett. **118**, 016602 (2017)].

[8] K. S. Zhuravlev, A. I. Toropov, T. S. Shamirzaev, and A. K. Bakarov, Photoluminescence of high-quality AlGaAs layers grown by molecular-beam epitaxy, Appl. Phys. Lett. **76**, 1131 (2000).

[9] A. Jasik, A. Wnuk, J. Gaca, M. Wójcik, A. Wójcik-Jedlińska, J. Muszalski, and W. Strupiński, The influence of the growth rate and V/III ratio on the crystal quality of InGaAs/GaAs QW structures grown by MBE and MOCVD methods, J. Cryst. Growth **311**, 4423 (2009).

[10] V. Srinivas, Y. J. Chen, and C. E. C. Wood, Reflectivity of two-dimensional polaritons in GaAs quantum wells, Phys. Rev. B **48**, 12300 (1993).

[11] S. V. Poltavtsev, Yu. P. Efimov, Yu. K. Dolgikh, S. A. Eliseev, V. V. Petrov, and V. V. Ovsyankin, Extremely low inhomogeneous broadening of exciton lines in shallow (In, Ga)As/GaAs quantum wells, Sol. St. Commun. **199**, 47 (2014).

[12] A. V. Trifonov, S. N. Korotan, A. S. Kurdyubov, I. Ya. Gerlovin, I. V. Ignatiev, Yu. P. Efimov, S. A. Eliseev, V. V. Petrov, Yu. K. Dolgikh, V. V. Ovsyankin, and A. V. Kavokin, Nontrivial relaxation dynamics of excitons in high-quality InGaAs/GaAs quantum wells, Phys. Rev. B **91**, 115307 (2015).

[13] E. S. Khramtsov, P. A. Belov, P. S. Grigoryev, I. V. Ignatiev, S. Yu. Verbin, Yu. P. Efimov, S. A. Eliseev, V. A. Lovtcius, V. V. Petrov, and S. L. Yakovlev, Radiative decay rate of excitons in square quantum wells: Microscopic modeling and experiment, J. Appl. Phys. **119**, 184301 (2016).

[14] P. S. Grigoryev, A. S. Kurdyubov, M. S. Kuznetsova, I. V. Ignatiev, Yu. P. Efimov, S. A. Eliseev, V. V. Petrov, V. A. Lovtcius, and P. Yu. Shapochkin, Excitons in asymmetric quantum wells, Superlatt. Microstruct. **97**, 452 (2016).

[15] E. S. Khramtsov, P. S. Grigoryev, D. K. Loginov, I. V. Ignatiev, Yu. P. Efimov, S. A. Eliseev, P. Yu. Shapochkin, E. L. Ivchenko, and M. Bayer, Exciton spectroscopy of optical reflection from wide quantum wells, Phys. Rev. B **99**, 035431 (2019).

[16] *Molecular Beam Epitaxy and Heterostructures*, edited by L. L. Chang and K. Ploog, NATO ASI Series Vol. 87 (1985).

[17] Marian A. Herman, W. Richter, and Helmut Sitter, *Epitaxy: Physical Principles and Technical Implementation* (Springer, Berlin Heidelberg, 2004), 525 p.

[18] P. Frigeri, L. Seravalli, G. Trevisi, and S. Franchi, Molecular beam epitaxy: An overview, Comprehensive Semicond. Sci. Techn. **3**, 480 (2011).

[19] J. W. Orton and T. Foxon, *Molecular Beam Epitaxy: A Short History* (Oxford University Press, Oxford, 2015).

[20] G. Bastard, E. E. Mendez, L. L. Chang, and L. Esaki, Exciton binding energy in quantum wells, Phys. Rev. B **26**, 1974 (1982).

[21] A. M. Fox, D. A. B. Miller, G. Livescu, J. E. Cunningham, and W. Y. Jan, Excitonic effects in coupled quantum wells, Phys. Rev. B **44**, 6231 (1991).

[22] B. Gerlach, J. Wuesthoff, M. O. Dzero, and M. A. Smondyrev, Exciton binding energy in a quantum well, Phys. Rev. B **58**, 10568 (1998).

[23] J. P. Prineas, C. Ell, E. S. Lee, G. Khitrova, H. M. Gibbs, and S. W. Koch, Exciton-polariton eigenmodes in light-coupled $In_{0.04}Ga_{0.96}As$/GaAs semiconductor multiple-quantum-well periodic structures, Phys. Rev. B **61**, 13863 (2000).

[24] E. L. Ivchenko, *Optical Spectroscopy of Semiconductor Nanostructures* (Springer-Verlag, Berlin Heidelberg, 2004).

[25] D. Schiumarini, N. Tomassini, L. Pilozzi, and A. D'Andrea, Polariton propagation in weak-confinement quantum wells, Phys. Rev. B **82**, 075303 (2010).

[26] H. M. Gibbs, G. Khitrova, and S. W. Koch, Exciton-polariton light-semiconductor coupling effects, Nat. Photonics **5**, 273 (2011).

[27] K. Sivalertporn, L. Mouchliadis, A. L. Ivanov, R. Philp, and E. A. Muljarov, Direct and indirect excitons in semiconductor coupled quantum wells in an applied electric field, Phys. Rev. B **85**, 045207 (2012).

[28] B. Jusserand, A. N. Poddubny, A. V. Poshakinskiy, A. Fainstein, and A. Lemaitre, Polariton Resonances for Ultrastrong Coupling Cavity Optomechanics in GaAs/AlAs Multiple Quantum Wells, Phys. Rev. Lett. **115**, 267402 (2015).

[29] S. I. Tsintzos, A. Tzimis, G. Stavrinidis, A. Trifonov, Z. Hatzopoulos, J. J. Baumberg, H. Ohadi, and P. G. Savvidis, Electrical Tuning of Nonlinearities in

Exciton-Polariton Condensates, Phys. Rev. Lett. **121**, 037401 (2018).

[30] A. V. Trifonov, E. S. Khramtsov, K. V. Kavokin, I. V. Ignatiev, A. V. Kavokin, Y. P. Efimov, S. A. Eliseev, P. Yu. Shapochkin, and M. Bayer, Nanosecond Spin Coherence Time of Nonradiative Excitons in GaAs/AlGaAs Quantum Wells, Phys. Rev. Lett. **122**, 147401 (2019).

[31] L. C. Andreani and A. Pasquarello, Accurate theory of excitons in GaAs $-$ $Ga_{1-x}Al_xAs$ quantum wells, Phys. Rev. B **42**, 8928 (1990).

[32] L. C. Andreani, Radiative lifetime of free excitons in quantum wells, Sol. St. Commun. **77**, 641 (1991).

[33] B. Deveaud, F. Clerot, N. Roy, K. Satzke, B. Sermage, and D. S. Katzer, Enhanced Radiative Recombination of Free Excitons in GaAs Quantum Wells, Phys. Rev. Lett. **67**, 2355 (1991).

[34] D. S. Citrin, Radiative lifetimes of excitons in quantum wells: Localization and phase-coherence effects, Phys. Rev. B **47**, 3832 (1993).

[35] R. C. Iotti and L. C. Andreani, Crossover from strong to weak confinement for excitons in shallow or narrow quantum wells, Phys. Rev. B **56**, 3922 (1997).

[36] A. D'Andrea, N. Tomassini, L. Ferrari, M. Righini, S. Selci, M. R. Bruni, D. Schiumarini, and M. G. Simeone, Optical properties of stepped $In_xGa_{1-x}As/GaAs$ quantum wells, J. Appl. Phys. **83**, 7920 (1998).

[37] M. M. Voronov, E. L. Ivchenko, V. A. Kosobukin, and A. N. Poddubnyi, Specific features in reflectance and absorbance spectra of one-dimensional resonant photonic crystals, Fiz. Tverd. Tela 49, 1709 (2007). [Phys. Solid State **49**, 1792 (2007)].

[38] E. L. Ivchenko, V. P. Kochereshko, A. V. Platonov, D. R. Yakovlev, A. Wang, B. Ossau, and G. Landwehr, Resonant optical spectroscopy of long-period quantum-well structures, Fiz. Tverd. Tela 39, 2072 (1997). [Phys. Solid State **39**, 1852 (1997)].

[39] I. Vurgaftman, J. R. Meyer, and L. R. Ram-Mohan, Band parameters for III–V compound semiconductors and their alloys, J. Appl. Phys. **89**, 5815 (2001).

[40] A. Askitopoulos, H. Ohadi, A. V. Kavokin, Z. Hatzopoulos, P. G. Savvidis, and P. G. Lagoudakis, Polariton condensation in an optically induced two-dimensional potential, Phys. Rev. B **88**, 041308(R) (2013).

[41] A. V. Trifonov, Yu. P. Efimov, S. A. Eliseev, V. A. Lovtcius, P. Yu. Shapochkin, and I. V. Ignatiev, Exciton scattering in heterostructures with (In, Ga)As/GaAs quantum wells, Bull. Russ. Acad. Sci.: Phys. **81**, 1481 (2017).

[42] The energies of the X_{hh} and X_{lh} excitons are calculated for separate QW widths, $L_{QW} = (8 + 3j)$ nm, with integer $j = 1, 2, \ldots$. The dependencies obtained are then approximated by a phenomenological function, $E_X(L) = a/L^\alpha + b$, with parameters $a = 1.62290$ eV, $b = 1.51085$ eV, $\alpha = 1.5678$ for the X_{hh} exciton, and $a = 1.73131$ eV, $b = 1.50829$ eV, $\alpha = 1.5422$ for the X_{lh} exciton.

[43] A. Tredicucci, Y. Chen, F. Bassani, J. Massies, C. Deparis, and G. Neu, Center-of-mass quantization of excitons and polariton interference in GaAs thin layers, Phys. Rev. B **47**, 10348 (1993).

[44] E. V. Ubyivovk, Yu. K. Dolgikh, Yu. P. Efimov, S. A. Eliseev, I. Ya. Gerlovin, I. V. Ignatiev, V. V. Petrov, and V. V. Ovsyankin, Spectroscopy of high-energy excitonic states in ultra-thick GaAs quantum wells with a perfect crystal structure, J. Lumin. **102**, 751 (2003).

[45] J. J. Davies, D. Wolverson, V. P. Kochereshko, A. V. Platonov, R. T. Cox, J. Cibert, H. Mariette, C. Bodin, C. Gourgon, I. V. Ignatiev, E. V. Ubylvovk, Yu. P. Efimov, and S. A. Eliseev, Motional Enhancement of Exciton Magnetic Moments in Zinc-blende Semiconductors, Phys. Rev. Lett. **97**, 187403 (2006).

[46] The heterostructure T683 also contains a narrow 14-nm QW; see Table VI. The respective exciton resonance is not shown in Fig. 8, because a similar exciton resonance is already discussed for the structure T798. It is useful, however, to present here the basic parameters of this resonance: $E_X = 1.52645$ eV, $\hbar\Gamma_0 = 29$ μeV, $\hbar\Gamma = 48$ μeV. The small nonradiative broadening indicates the high quality of this structure.

[47] P. S. Grigoryev, O. A. Yugov, S. A. Eliseev, Yu. P. Efimov, V. A. Lovtcius, V. V. Petrov, V. F. Sapega, and I. V. Ignatiev, Inversion of Zeeman splitting of exciton states in InGaAs quantum wells, Phys. Rev. B **93**, 205425 (2016).

[48] A. D. Bristow, T. Zhang, M. E. Siemens, S. T. Cundiff, and R. P. Mirin, Separating homogeneous and inhomogeneous line widths of heavy- and light-hole excitons in weakly disordered semiconductor quantum wells, J. Phys. Chem. B **115**, 5365 (2011).

[49] www.photon.spbu.ru